Advanced Electronic Materials

ADVANCED ELECTRONIC MATERIALS

www.advelectronicmat.de

RESEARCH ARTICLE OPEN ACCESS

Structural and Electrical Behavior of Swift Heavy Ion Irradiated Hafnium Oxide Polymorphs in Ferroelectric and Resistive Memories

Philipp Schreyer[1] | David Lehninger[2] | Tobias Vogel[1] | Tianren Zhang[2] | Taewook Kim[1] | Eszter Piros[1] | Yingxin Li[1] | Yu Duan[1] | Maximilian Lederer[2] | Konrad Seidel[2] | Christina Trautmann[1,3] | Eugenia Toimil-Molares[1,3] | Lambert Alff[1]

[1]Advanced Thin Film Technology Division, Institute of Materials Science, Technische Universität Darmstadt, Darmstadt, Germany | [2]Fraunhofer IMPS, Center Nanoelectronic Technologies (CNT), Dresden, Germany | [3]Institute of Materials Science, GSI Helmholtzzentrum für Schwerionenforschung, Darmstadt, Germany

Correspondence: Philipp Schreyer (Philipp.schreyer@tu-darmstadt.de)

Received: 11 September 2025 | **Revised:** 13 November 2025 | **Accepted:** 25 November 2025

Keywords: energy loss threshold | hafnium oxide | meta-insulator-metal capacitors | resistive random-access memories | swift heavy-ion irradiation

ABSTRACT

Hafnium oxide (HfO_2) exhibits multiple polymorphs, each with distinct properties and is a promising material for non-volatile memory technologies in radiation-harsh environments. To gain a comprehensive understanding of the radiation response of HfO_2-based memory devices requires detailed investigations of ion beam-induced phase changes as well as, recrystallization processes and amorphization in the different HfO_2 polymorphs. This study explores the effects of swift heavy-ion irradiation on HfO_2 in resistive random-access memories (RRAM) and metal-insulator-metal (MFM) capacitors, using 1.635 GeV Au ions, to simulate an extreme damage scenario, and 183 MeV Ca ions, which are more relevant to space missions due to their lower mass. The exposure of RRAM layers and MFM capacitors to Ca ions has a negligible effect on the crystallinity of HfO_2 with little to no impact on the switching behavior of the capacitors, indicating that the energy loss threshold for inducing phase transitions is not exceeded. Comparing La-doped HfO_2 (HLO) and hafnium zirconium oxide (HZO) MFM capacitors reveals that HZO exhibits remarkable resilience against Au ion irradiation up to fluences of 7×10^{12} ions/cm^2, without any reduction in saturation polarization and that the ferroelectric properties of HLO and HZO can be restored and even enhanced through post-irradiation cycling.

1 | Introduction

The continuous progress in artificial intelligence (AI) has led to a growing interest in technologies that mimic the complexity of the human brain, notably neuronal networks. Non-volatile memories such as oxide-based random-access memories (OxRAM) [1–5] or ferroelectric-random-access memories (FeRAM) [6–8], ferroelectric tunnel junctions (FTJ) [9], ferroelectric metal field effect transistors (FeMFET) [9] and ferroelectric field effect transistors (FeFET) [10–12] based on complementary metal-oxide semiconductor (CMOS) compatible hafnium oxide, are potential candidates for next-generation non-volatile memory technologies [13–16]. These memory types could play a crucial role in the development of future neuromorphic computing systems. As AI becomes more integrated into everyday technologies and specialized applications including fields such as healthcare, transportation, aerospace and space missions, the associated data storage, in particular non-volatile memories, must be capable of withstanding harsh environments, such as exposure to ionizing radiation.

Conventional CMOS-based memory technologies, such as dynamic random-access memory (DRAM), static random-access memory (SRAM) and flash memory, rely on charge-based mechanisms to store information. Consequently, they are inherently susceptible to radiation-induced effects and defects [17] including single-event upsets (SEUs), single-event latch-ups or single-event functional interruptions (SEFIs) which can compromise data integrity and system reliability [18].

In contrast, the operating principles of non-volatile memories, such as resistive random-access memories (RRAM) and FeRAM, are markedly distinct from those of charge-based memories as their memory storage mechanisms are strongly influenced by defects (e.g., oxygen vacancies), ion migration and the crystal structure of the switching material. This results in a notably enhanced resilience to radiation [6, 19–21]. The enhanced radiation tolerance has been demonstrated in multiple studies on hafnium oxide [19, 21–25] exposed to various forms of irradiation, including X-rays [23], protons [26–29], gamma radiation [22, 30], and heavy ions [31, 32].

As previously outlined, oxygen vacancies have been shown to play a substantial role in the switching behavior of oxide-based RRAM and metal-insulator-metal (MFM) capacitors which are an essential component of ferroelectric devices. A FeRAM memory cell can be created by connecting the capacitor to the drain contact of a transistor or to the gate if it is connected to a FeMFET [9]. It has been demonstrated that the interaction of ions with preexisting vacancies in HfO_2 results in the creation of additional oxygen vacancies [19]. Even a small increase in the oxygen vacancy concentration can induce a complete change in the RRAM switching behavior [33–35].

Another significant phenomenon that arises under ion irradiation is phase transformation, which occurs when a specific energy loss of the ions surpasses a critical threshold and a sufficiently high fluence is exceeded. Benyagoub et al. reported that monoclinic hafnium oxide grains can undergo a phase transition to the tetragonal phase when the electronic energy loss exceeds 18 keV/nm [36–39]. This phase transition is attributed to the formation of overlapping ion tracks [40] produced via inelastic thermal spikes [41, 42]. The initial ions create tracks with oxygen vacancies around their trajectories. With increasing fluence, the probability of subsequent ions interacting with the pre-damaged track zones rises, ultimately leading to a macroscopic phase transition. This process is referred to as the double-hit phase transition process.

In earlier studies, we demonstrated that oxygen vacancies alone are capable of inducing a transition to the cubic phase with a rhombohedral distortion in highly textured hafnium oxide films [43]. This transformation was confirmed by 4D scanning transmission electron microscopy on initially monoclinic HfO_2 films irradiated with 1.6 GeV Au ions [19]. Furthermore, automated crystal orientation mapping revealed that heavy ion-induced phase transitions can be accompanied by grain fragmentation [19]. Such grain fragmentation may be falsely attributed to amorphization in X-ray diffraction (XRD) analyses, as nanocrystalline grains remain undetectable by XRD alone.

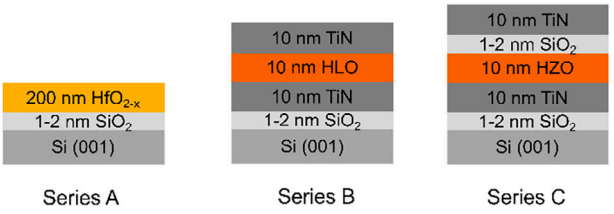

FIGURE 1 | Schematic overview of sample series (A), (B) and (C) each with different hafnium oxide and electrode layer configurations. The fabrication details and stack compositions are described in the main text.

In ferroelectric hafnium-zirconium-oxide devices, structural alterations induced by swift heavy ion irradiation have been directly correlated with changes in electrical performance. Following irradiation, a reduced remanent polarization was observed and attributed to the loss of the polar orthorhombic phase. It has also been shown that electric field cycling after irradiation can recover and even enhance the ferroelectric behavior by electric-field induced phase transitions back to the polar orthorhombic phase [6, 19, 44]. These findings demonstrate the complex interplay between different hafnium oxide polymorphs, ion irradiation and electrical properties.

To gain a more comprehensive understanding of the subject, the present study investigates the interaction of both amorphous and crystalline hafnium oxide, each containing different oxygen concentrations, with 1.635 GeV gold ions and 0.183 GeV Ca ions at various fluences. Furthermore, MFM capacitors based on lanthanum-doped HfO_2 (HLO) and hafnium zirconium oxide (HZO) were irradiated. In this case, a systematic characterization of remanent and spontaneous polarizations, along with post-irradiation voltage-dependent polarization (P−V) cycling, was conducted and complemented by structural investigations.

2 | Experimental

Three different sample series of hafnium oxide-based layers (indexed as A, B and C) were investigated. A schematic overview of all sample series is presented in Figure 1.

The samples of series A consist of 200 nm thick full-sheet HfO_2 layers deposited on a Si substrate by molecular beam evaporation. Metallic hafnium was evaporated onto a Si(100) substrate at room temperature to produce an amorphous film and at 320°C for crystalline samples using a controlled flux of oxygen radicals and a plasma power of 200 and 280 W, respectively. The oxygen content of the films was controlled in situ during film growth by adjusting the oxygen gas flow, the radio-frequency (RF) power of the plasma, and the evaporation rate of the hafnium source. In this way, oxygen-deficient as well as stoichiometric amorphous and crystalline hafnium oxide samples were produced.

Samples of series B consist of a 10 nm thick layer of HLO grown via atomic layer deposition (ALD) onto a 10 nm TiN bottom electrode on a highly boron-doped Si substrate. The cycling ratio of La:Hf was 1:15, leading to a doping concentration of approximately 6.25%

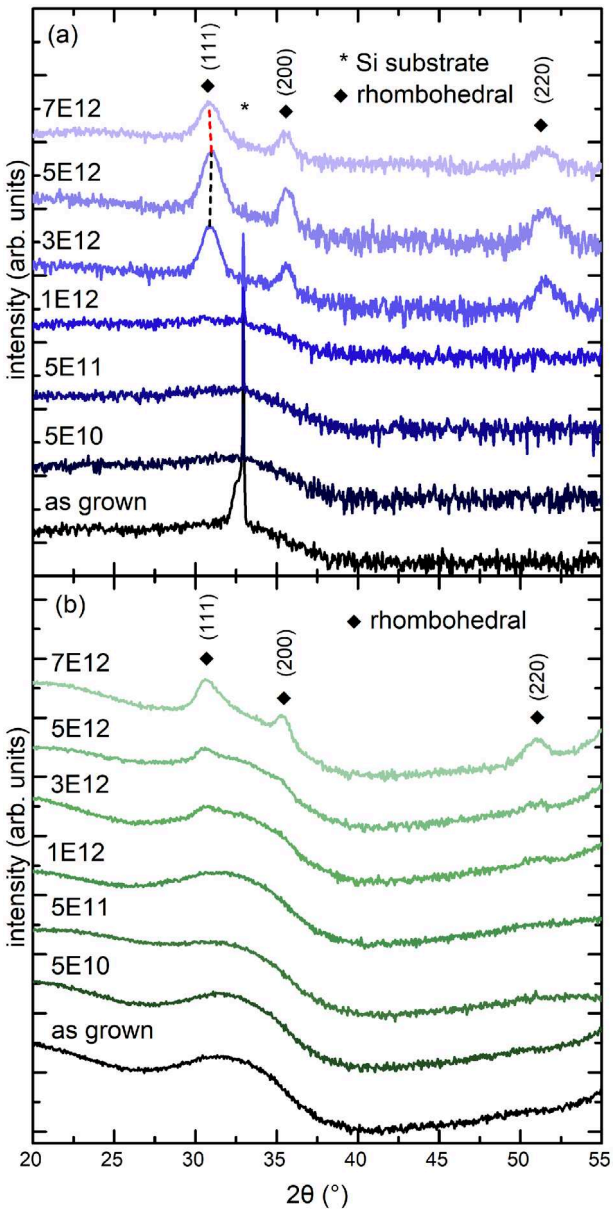

FIGURE 2 | XRD 2θ–ω patterns of as grown and Au ion irradiated amorphous films (sample series A) at fluences from 5×10^{10} to 7×10^{12} ions/cm^2, revealing ion-beam induced crystallization to a rhombohedral phase for (a) a sub-stoichiometric oxygen-deficient HfO_{2-x} layer measured in the 2θ–ω geometry and (b) a stoichiometric HfO_2 layer measured with GIXRD. Reflections of the rhombohedral phase are marked with ◆. The forbidden 200 silicon reflection originating from the substrate is marked with *.

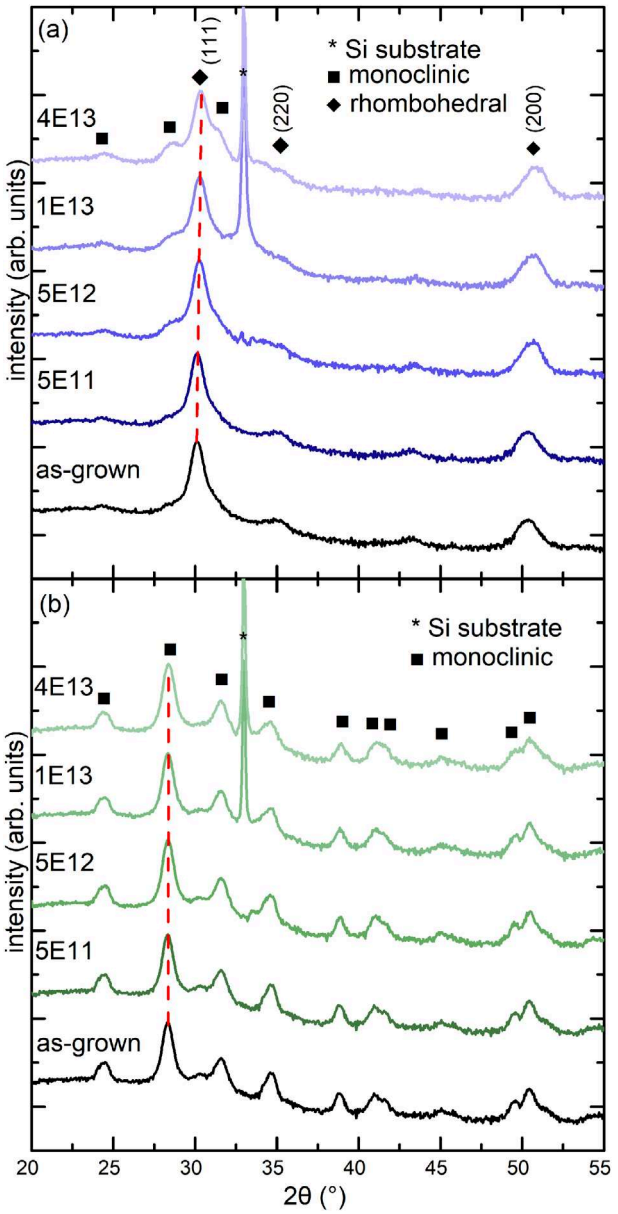

FIGURE 3 | XRD 2θ–ω patterns of crystalline hafnium oxide samples irradiated with 183 MeV Ca ions at fluences from 5×10^{11} to 4×10^{13} ions/cm^2. (a) Oxygen-deficient HfO_{2-x} films revealing an increase in monoclinic phase and a slight shift of the rhombohedral reflection toward higher angles with increasing fluence. (b) Stoichiometric HfO_2 films showing no phase transition across all fluences. Reflections of the rhombohedral phase are marked with ◆ and reflections of the monoclinic phase are marked with ■. The forbidden 200 reflection of the silicon substrate is marked with *.

of La. The TiN bottom electrode was also fabricated via ALD using NH_3 and $TiCl_4$ as precursors at a temperature of 450°C. To avoid in situ crystallization of the doped HLO layer, the TiN top electrode was sputtered at room temperatures.

Samples of series C consist of 10 nm HZO grown by ALD on a 10 nm TiN bottom electrode on a Si substrate. Bottom and top TiN electrodes in this series were grown in the same way as in series B, by ALD and sputtering respectively. The 10 nm HZO films were produced by ALD using $HfCl_4$ and $ZrCl_4$ precursors with a 1:1 cycling ratio to obtain $Hf_{0.5}Zr_{0.5}O_2$. To achieve the desired ferroelectric orthorhombic phase both HZO and HLO samples underwent furnace annealing at 400°C for 1 h after deposition. The SiO_2 layer between HZO and top electrode was grown in a wet-chemical process.

Heavy ion irradiation experiments were carried out at the X0- and M3-beam lines of the UNILAC accelerator at the GSI Helmholtzzentrum für Schwerionenforschung in Darmstadt, Germany. The samples were irradiated with 1.635 GeV Au and 0.183 GeV Ca ions. The respective ranges of the ions are 34.4 µm

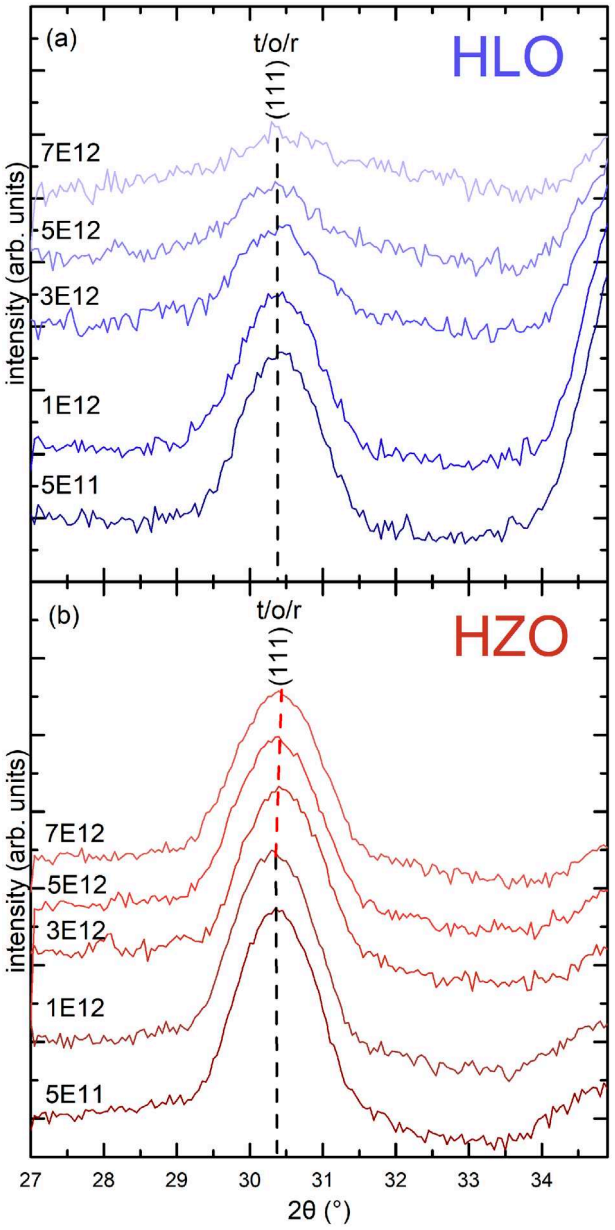

FIGURE 4 | XRD 2θ–ω patterns of the 111 tetragonal, orthorhombic or rhombohedral phases of (a) HLO and (b) HZO irradiated with Au ions at fluences ranging from 5×10^{11} to 7×10^{12} ions/cm^2. For HLO the peak shape and intensity changes at and above a fluence of 3×10^{12} ions/cm^2. For HZO a slight shift of the 111 reflection occurs accompanied by peak broadening.

(Au) and 16.8 μm (Ca) which, in both cases, are much larger than the thickness of the stacked film samples (the ions thus stop deep in the Si substrate). The applied fluences ranged from 5×10^9–7×10^{12} ions/cm^2 for Au and 5×10^{11}–4×10^{13} ions/cm^2 for Ca. The estimated uncertainty of the ion fluence is in the order of 10 – 20%. To minimize thermal effects during irradiation, the flux of the ion beam was limited to approximately 5×10^8 ions/cm^{2}s. During irradiation, no external bias was applied to the samples.

XRD measurements were performed with a Rigaku Smartlab system in parallel beam configuration using Cu $K_{\alpha 1}$ radiation from a rotating anode source. For 2θ–ω scans a Ge(220) double bounce monochromator was used. For the analyses of very thin films (10 nm and less) grazing incidence X-ray diffraction (GIXRD) with Soller slits with a width of 5 mm was employed to enhance signal intensity.

To evaluate the electrical characteristics of the MFM capacitors, circular Ti/Pt top electrodes were deposited via electron beam evaporation through a shadow mask. A subsequent wet etching process removed the excess material of the TiN top electrode between the dot contacts, resulting in isolated MFM capacitors with areas ranging from 0.150 to 0.006 mm^2. Electrical programming and testing were conducted on a Cascade Microtech probe station with an Agilent B1500 parameter analyzer. P–V hysteresis loops were measured using an Aixacct TF 3000 FE analyzer with a triangular waveform at 1 kHz. Electric field cycling was performed at a fixed frequency of 1 kHz, applying a field strength of 3 MV/cm. The highly doped silicon wafers served as the bottom (ground) electrode. Five different devices were tested for HLO and HZO respectively.

3 | Results and Discussion

3.1 | Response of Amorphous Hafnium Oxide Full Sheet Layers for RRAM Applications to Au and Ca Ion Irradiation

3.1.1 | Effect of Heavy Au Ion Irradiation on Amorphous Hafnium Oxide Films with Different Oxygen Content

In this section the effects of the Au ion irradiation on amorphous hafnium oxide films with different oxygen contents (see Figure 1 sample series A) are studied. The present study focuses on the response of amorphous HfO_2 to Au-ion irradiation extending our previous investigation on crystalline HfO_2 with varying stoichiometries [19, 20]. Figure 2a presents the XRD patterns of amorphous sub-stoichiometric HfO_{2-x} films, irradiated at fluences ranging from 5×10^{10} to 7×10^{12} ions/cm^2 along with the data of the as-grown film (black curve) for comparison. With increasing fluence, there is a noticeable crystallization of a defect-stabilized rhombohedral phase. Initially identified as a cubic low-temperature phase (LTP), this phase was recently discussed in detail by Kaiser et al. and reinterpreted as a defect-stabilized rhombohedral phase, derived from the cubic phase by a slight distortion along the [111] direction (distorted Fm3m, ICCD: 04-011-9018) [43, 45]. Crystallization becomes evident at fluences higher than 1×10^{12} ions/cm^2 with the first reflections appearing at 3×10^{12} ions/cm^2. The most prominent reflection from the 111 lattice plane occurs at $2\theta \approx 30.57°$ as expected for the rhombohedral phase. As a result of the ion-beam induced crystallization, there is no texture transfer from the substrate. This leads to polycrystalline grain growth, which is visible from the appearance of additional 200 and 220 reflections. The contribution of the rhombohedral phase increases up to a fluence of 5×10^{12} ions/cm^2. The substrate reflection around $2\theta \approx 32$–$34°$ corresponds to the forbidden 200 Si reflection (Umweganregung) [46]. The intensity and shape of this reflection changes with the in-plane position (Φ angle, i.e., the horizontal planar rotation angle of the sample). By adjusting the Φ-angle, this reflection is typically completely avoided.

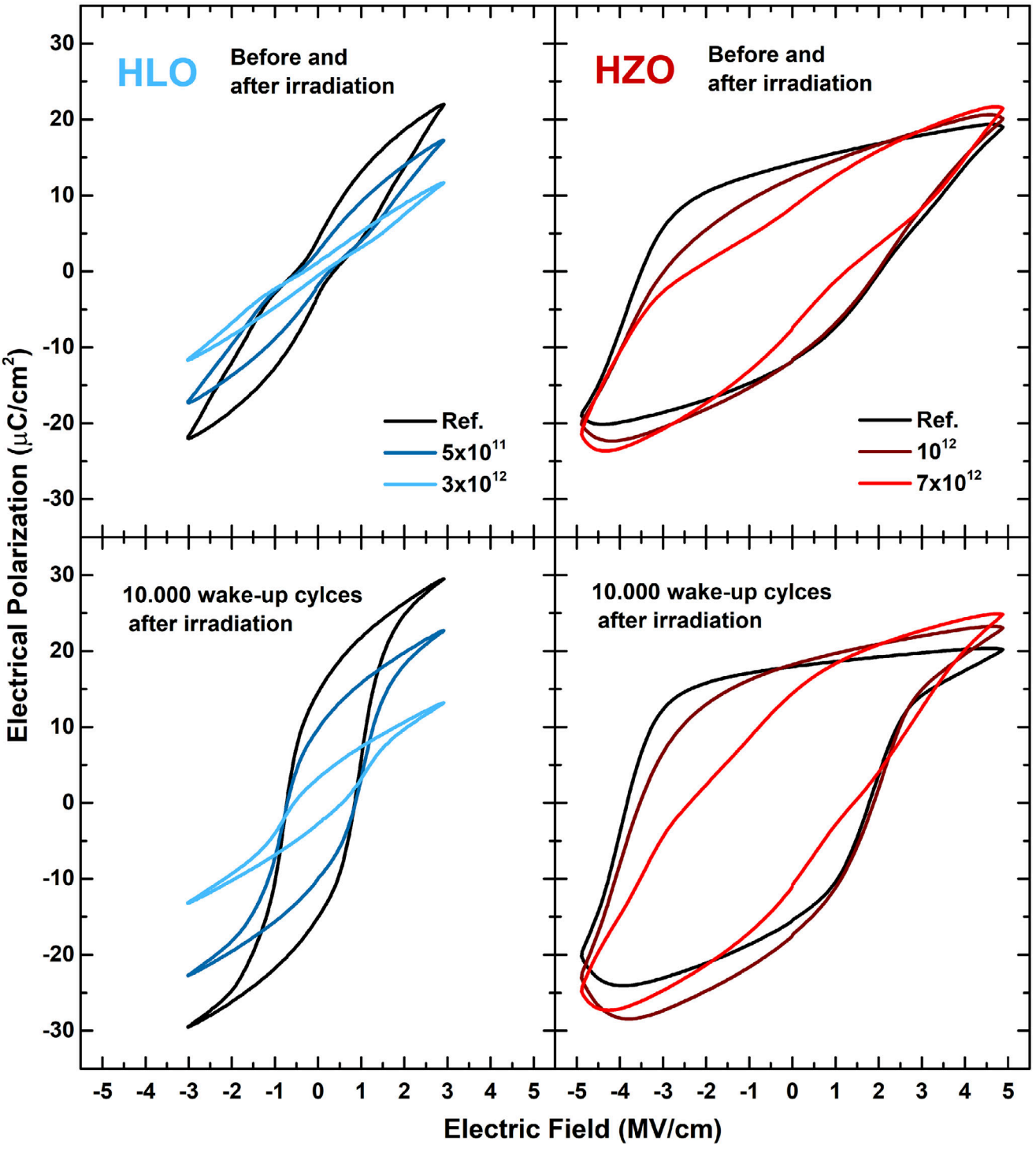

FIGURE 5 | (Top) Electrical polarization hysteresis loops of HLO and HZO before and after irradiation with Au ions at two fluences (given in ions/cm^2) compared to a non-irradiated reference sample. The HZO stack exhibits asymmetrical polarization loops due to the additional SiO_2 layer between HZO and top electrode. (Bottom) Hysteresis loops after 10.000 cycles for the same fluences compared to the non-irradiated reference sample showing wake-up behavior.

The explanation for the observed crystallization process at higher fluences is not straightforward. We can rule out macroscopic sample heating, as the ion flux was limited and the estimated sample temperature was between 50–60°C, well below the crystallization temperature of HfO_2. However, at the microscopic level, each ion that penetrates through the sample deposits an enormous amount of energy along its trajectory. According to the so-called inelastic thermal spike model [47, 48], the formation of ion tracks involves short-term local melting of a nanometer-sized cylindrical region. Rapid cooling then freezes the molten track cylinder into a defect-rich or amorphous track. In hafnium oxide, this process may lead to complete or partial recrystallization. Based on our XRD data, crystallization begins at fluences above 1×10^{12} ions/cm^2, where ion tracks start to overlap significantly.

TABLE 1 | Remanent (P_R) and saturation (P_S) polarization of HLO and HZO at various fluences of Au ion irradiation before and after 10.000 cycles.

Material	Fluence (ions/cm²)	Condition	P_R (μC/cm²)	P_S (μC/cm²)
HLO	Reference	Pristine	4.7	22.0
		After 10^4 Cycles	14.6	29.5
	5×10^{11}	Pristine	3.1	17.3
		After 10^4 cycles	9.8	22.7
	3×10^{12}	Pristine	1.3	11.5
		After 10^4 Cycles	3.4	13.1
HZO	Reference	Pristine	14.4	19.1
		After 10^4 Cycles	18.2	20.2
	5×10^{11}	Pristine	12.2	20.0
		After 10^4 cycles	18.2	23.1
	3×10^{12}	Pristine	8.3	21.7
		After 10^4 Cycles	14.5	25

The process is likely driven by a double-hit mechanism which requires a pre-damaged state. Given that the amorphous film was oxygen-deficient before irradiation, it is likely that crystallization directly to the rhombohedral phase occurred, as a substantial number of oxygen vacancies were introduced during film growth, promoting the crystallization of the rhombohedral phase. It is noteworthy that the position of the reflection at $2\theta = 30.94°$ for a fluence of 3×10^{12} ions/cm² is at a slightly higher angle than that of an as-grown rhombohedral sample ($2\theta = 30.57°$) [43]. This suggests that a considerable number of additional oxygen vacancies were already created at lower fluences even before the crystallization of the amorphous film began. With increasing fluence, the amount of oxygen vacancies increases as each ion impact produces extra defects which in turn shifts the 111 reflection to higher angles. However, at a fluence of 7×10^{12} ions/cm², the intensity of the reflection decreases slightly and the reflection broadens (FWHM = 1.4° at 7×10^{12} ions/cm² compared to FWHM = 1.23° at 5×10^{12} ions/cm²). In a previous study, we demonstrated that the reduction in intensity at higher fluences is due to grain fragmentation without amorphization [19, 20]. In addition, the broadening can be attributed to either a reduction in grain size or an increase in the number of defects, which may result in a variation in the lattice constant and the formation of different suboxide phases of HfO_{2-x}. Furthermore, it is evident that the 111 reflection initially shifts to higher angles (see black dashed line in Figure 2a and then, at a fluence of 7×10^{12} ions/cm², returns to lower angles (see red dashed line in Figure 2a. This behavior contrasts with previous studies [19, 20], where the reflection consistently moved to larger angles with higher fluences, which was attributed to an increased number of oxygen vacancies caused by the ion irradiation.

To rule out the possibility of experimental errors (e.g., beam inhomogeneities), additional data of crystalline rhombohedral HfO_{2-x} layers is presented in Figure S1. These samples were irradiated in the same run and on the same sample holder but do not show a shift to lower angles at 7×10^{12} ions/cm². The underlying reason for this phenomenon could stem from the distinct microstructures and stress states of amorphous and crystalline layers. Subsequent to the initial crystallization, amorphous layers usually exhibit elevated residual stresses and a heterogeneous distribution of defects. At moderate fluences, the creation of oxygen vacancies results in a contraction of the crystal lattice and an increase in the 2θ value. However, as the fluence increases further, vacancy defects may cluster, forming tiny voids, causing the layer to expand locally and residual stresses to relax partially. This leads to an increase in the out-of-plane lattice spacing and a reduction in the 2θ value. Existing literature demonstrates that the introduction of stress in amorphous material is influenced by their growth process and defects due to ion bombardment. Both effects can lead to an initial increase in stress and potential stress relaxation [49]. This behavior is distinct from that of crystalline materials, which tend to maintain higher stress levels due to constraints imposed by their crystalline structure.

Figure 2b shows the GIXRD patterns of the stoichiometric amorphous HfO_2 samples (see Figure 1 sample series A), irradiated at fluences ranging from 5×10^{10} to 7×10^{12} ions/cm². Also, for these films, the rhombohedral phase emerges at a fluence of 3×10^{12} ions/cm². This crystallization behavior is unexpected for stoichiometric HfO_2 which typically crystallizes into the monoclinic phase before undergoing a crystalline-to-crystalline phase transition at higher fluences, as reported in the literature [19, 20, 38]. However, our data clearly indicate that the films not only crystallize directly but also transition into a sub-stoichiometric rhombohedral HfO_{2-x} phase. We propose that this direct phase transition to the rhombohedral phase is facilitated by the introduction of additional oxygen vacancies created during irradiation. According to Benyagoub et al. [38], the beam-induced phase transition requires a critical electronic stopping power threshold of 18 keV/nm and fluences high enough to produce overlapping tracks. Based on calculations with the SRIM-2013 code [50], the energy loss in HfO_2 (density 9.68 g/cm³ [51]) is 53 keV/nm. Thus, both threshold and fluence conditions are fulfilled for a phase transition at a fluence of 3×10^{12} ions/cm² [19, 38]. When comparing these samples with the oxygen-deficient amorphous films (Figure 2a), it is evident that although both samples crystallize into the rhombohedral phase, the reduced oxygen content in HfO_{2-x} leads to slightly higher 2θ angles ($2\theta = 30.84°$ compared to $2\theta = 30.74°$). Additionally, the

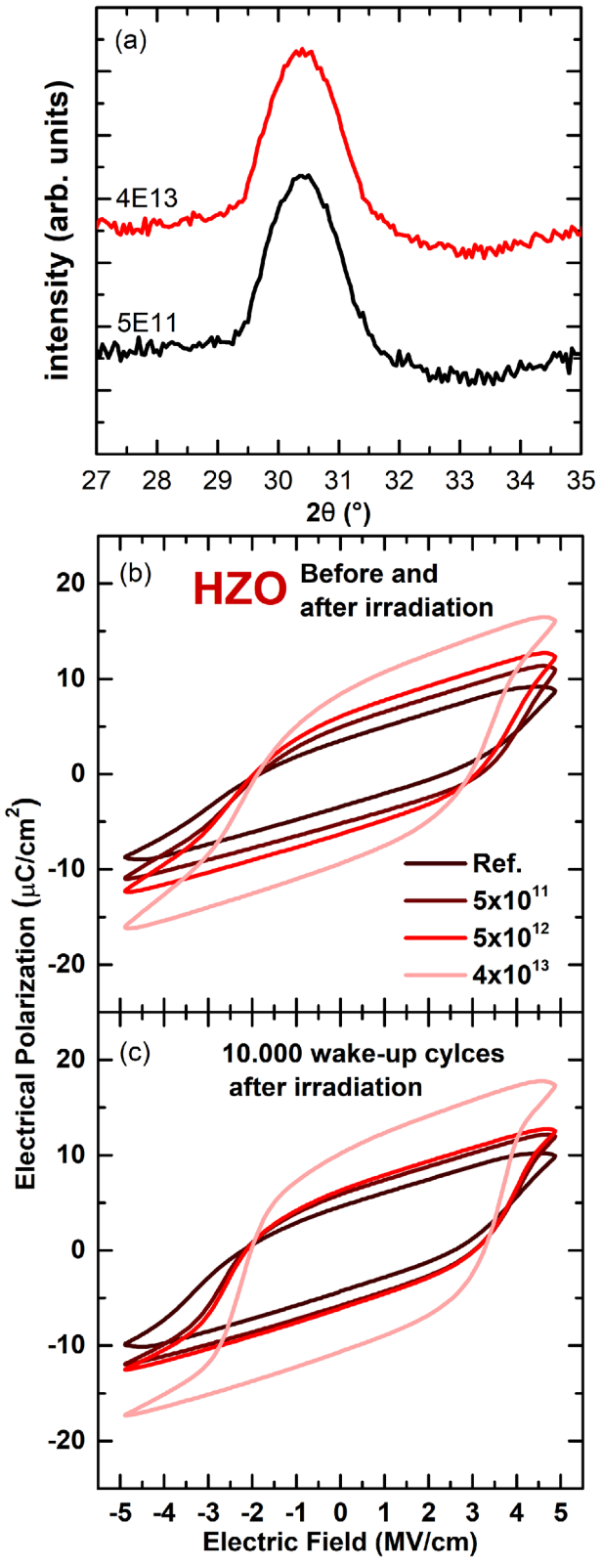

FIGURE 6 | (a) 2θ–ω XRD patterns of HZO for irradiation with Ca ions with low and high fluences. (b) Electrical polarization hysteresis loops of HZO before and after irradiation with Ca ions for three fluences (given in ions/cm^2) compared to a non-irradiated reference sample. (c) P–V loops after 10.000 cycles for the three fluences in (b) compared to the reference samples.

crystallin fraction of the rhombohedral phase in the irradiated stoichiometric samples is significantly lower than in the sub-stoichiometric samples. To provide a more accurate comparison of the relative intensities of the two amorphous samples, the 2θ–ω scan of the stoichiometric sample is included in Figure S2. This scan confirms that the intensities are notably weaker compared to those of the sub-stoichiometric sample. Vogel et al. have shown, that although the intensity of the rhombohedral reflection drops at higher fluences, there is no amorphization but rather an irradiation-induced grain fragmentation, a mechanism which may also explain our observations [19]. The results align with trends reported for irradiated crystalline hafnium oxide and highlight the remarkable resilience of rhombohedral HfO_{2-x} to swift heavy ion irradiation.

3.1.2 | Effect of Ca Ion Irradiation on Hafnium Oxide Films with Different Oxygen Content

In this section, we examine the radiation effects induced with 183 MeV Ca ions on crystalline hafnium oxide films with different oxygen contents. Compared to the irradiation with Au ions, less severe effects are expected because the electronic energy loss of Ca ions is only 10 keV/nm [50] thus much lower. To compensate for this reduced energy deposition, the maximum applied fluence of Ca ions was higher by a factor of ≈6 compared to the irradiation with Au ions. Figure 3 presents the XRD patterns of oxygen-deficient and stoichiometric crystalline hafnium oxide, irradiated with Ca ions of fluences ranging from 5×10^{11} to 4×10^{13} ions/cm^2. The XRD patterns of oxygen-deficient HfO_{2-x} (Figure 3a) reveals a minor component of the monoclinic phase. Across all fluences up to 4×10^{13} ions/cm^2, the reflections associated with the rhombohedral phase exhibit no significant change in peak shape. For the 111 reflections, we observe a slight shift toward larger angles (see red dashed line), increasing from 30.11° at the lowest fluence to 30.33° at the highest fluence. This shift suggests that oxygen vacancies are created in the film even with the lighter Ca ions despite their energy loss being considerably below the threshold of 18 keV/nm [38] required for phase transitions. With increasing fluence, the fraction of the monoclinic phase increases, while the fraction of the rhombohedral phase remains relatively constant. Obviously, a direct phase transition from the rhombohedral to the monoclinic phase does not occur under these irradiation conditions. A more detailed examination of the XRD pattern of the rhombohedral phase (see Figure 3a) at the lowest fluence level reveals the presence of a minor monoclinic phase component, particularly in the 110 plane at 24.18° and the -111 plane at 28.33°. As the fluence increases, the intensity of these reflections rises and at 4×10^{13} ions/cm^2, the 111 reflection of the monoclinic phase emerges. This observation suggests that some parts of the film were probably amorphous and stoichiometric after growth. At higher fluences where ion tracks significantly overlap, crystallization of these amorphous regions may occur This is in line with previous findings, where the energy loss threshold for crystallization of thin amorphous HfO_2 films was reported to be 10 keV/nm [52]. However, in contrast to the irradiation with Au ions, this phase remained in the monoclinic phase, indicating that the Ca ions did not deposit sufficient energy

to overcome the phase transition threshold, but still sufficient to initiate a crystallization process.

Figure 3b illustrates the response of stoichiometric monoclinic HfO_2 films to Ca ion irradiation. Even at the highest fluence of 4×10^{13} ions/cm^2, the phase remains rather unaffected with only minor variations in the shape of the reflections probably due to defect creation and increased mosaicity. The limited extend of radiation damage is indicated by the absence of a shift in the main -111 reflection (see red dashed line). As already noted, the Ca ions do not deposit sufficient energy to initiate a phase transition, explaining the absence of the rhombohedral phase, in contrast to irradiation with Au ions. This underscores the necessity of exceeding a specific energy loss threshold to trigger such a phase transition. Our results demonstrate that hafnium oxide films, irrespective of their crystal structure and stoichiometry, are well-suited for applications in memristive devices operating in cosmic radiation environments, which are dominated by protons and few light ions.

3.2 | Response of Hafnium-Zirconium-Oxide and La:HfO2 MFM Capacitors to Ca and Au Ion Irradiation and the Influence on their Ferroelectric Properties

In this section the effects of Ca and Au ion irradiation on the ferroelectric properties of HLO (Figure 1 sample series B) and HZO MFM capacitors (Figure 1 sample series C) are analyzed. The XRD patterns of Au-ion irradiated HLO and HZO (see Figure 4) both exhibit the characteristic 111 reflection of the tetragonal, rhombohedral or the non-centrosymmetric orthorhombic ferroelectric phase (space group $Pca2_1$; ICDD: 04-004-5597). As both samples exhibit ferroelectric properties, it can be concluded that the majority of the material crystallized in the orthorhombic phase. Therefore, these 111 reflections are assigned to this phase in the following. In HLO, the orthorhombic phase is preserved up to a fluence of 1×10^{12} ions/cm^2. At a fluence of 3×10^{12} ions/cm^2, the intensity of the orthorhombic 111 reflection at $2\theta = 30.4°$ decreases and it nearly disappears at 7×10^{12} ions/cm^2. Moreover, at 3×10^{12} ions/cm^2, the reflections become visibly broader, which we attribute to beam-induced defects, mainly oxygen vacancies which are known to be responsible for grain fragmentations or phase transitions [6, 19, 20]. While a pronounced intensity decrease and broadening of the reflections is often attributed to amorphization, prior studies (e.g., Vogel et al.) demonstrated that nanocrystalline grains may persist but are undetectable through XRD analysis alone [19, 53]. A similar trend, though less pronounced, is observed in the HZO stacks. Again, at 3×10^{12} ions/cm^2, a minor decrease in intensity of the 111 reflection is accompanied by a slight broadening and a shift of the reflection to larger angles (see red dashed line). However, even at 7×10^{12} ions/cm^2 the 111 reflection is still clearly visible indicating that just a small fraction of the ferroelectric orthorhombic phase has undergone grain fragmentation or transition to another phase.

Figure 5 presents polarization curves, i.e., the $P-V$ characteristics of HLO and HZO for different Au ion fluences, both for the initial cycle and after 10.000 cycles. A distinct asymmetrical polarization curve is exhibited by HZO due to the presence of an additional SiO_2 layer between HZO and the top electrode. For HLO, the irradiation with 5×10^{11} ions/cm^2 and above leads to a more pronounced pinching of the $P-E$ loops, accompanied by a gradual reduction in remanent (P_R) and saturation polarization (P_S). This behavior can be ascribed to antiferroelectric characteristics, which have been attributed in the literature to the presence of a tetragonal phase [54]. As the fluence increases, a large fraction of the polar orthorhombic phase transforms into a non-polar phase, resulting in enhanced pinching of the hysteresis loops. During film growth, it is likely that HfO_2 crystallised in both tetragonal and orthorhombic phases. However, as both phases exhibit very similar lattice constants, it is nearly impossible to distinguish between these phases in polycrystalline films. For both HLO and HZO, the P_R and P_S values before and after irradiation are shown in Table 1. At fluences exceeding 3×10^{12} ions/cm^2, the loops display dielectric behavior. This correlates well with our XRD results and the significant intensity decrease in the 111 reflection starting at the same fluence. HZO exhibits a similar trend but shows markedly greater resilience to the irradiation. Pinching of the loops, accompanied by a reduction in P_R, begins at fluences of 3×10^{12} ions/cm^2. However, even at the highest fluence studied, HZO still retains notable P_R and P_S values with P_S remaining nearly unaltered. For both samples, a reduction in the slope of the loops is observed with increasing fluence, indicating a decrease in symmetry, most likely due to an increased number of defects or grain boundaries. For HZO, the effects occur at considerably higher fluences suggesting a larger disordered volume within the ferroelectric layer which can be ascribed to grain fragmentation. The decline in P_S of HLO can be attributed to a loss of the switchable polar orthorhombic phase as a consequence of phase transitions to non-polar phases, such as the cubic or tetragonal phase [19], due to the generation of oxygen vacancies. In contrast, HZO shows a very slight increase in P_S leading to the conclusion that a smaller fraction of the ferroelectric phase is transitioned to a non-polar phase. Interestingly, in both samples the pinched P–V loops reopen after multiple cycling. Figure 5 shows that the initial P_R and P_S values recover after 10.000 cycles, indicating that both the HLO samples irradiated with 3×10^{12} ions/cm^2 as well as the HZO samples irradiated wit 7×10^{12} ions/cm^2 restore the polar phase suggesting a non-polar to polar phase transition from the potential antiferroelectric tetragonal phase to the ferroelectric orthorhombic phase.

It has previously been shown that La doping significantly reduces the formation energy of oxygen vacancies in HfO_2, resulting in a higher concentration of them in as-grown HLO compared to as-grown HZO [55, 56]. Furthermore, oxygen vacancies have been reported to drive the phase transition from the monoclinic to the rhombohedral and eventually to the hexagonal phase in HfO_2 [43, 45]. This mechanism has also been identified as the cause of ion-beam induced phase transitions [19]. We thus assume that this behavior is enhanced in the HLO sample rendering the sample more susceptible to irradiation than HZO.

Figure 6 presents the 2θ–ω XRD patterns and P–V characteristics of HZO films (Figure 1 sample series C) irradiated with Ca ions. In Table 2 both P_R and P_S values are presented before and after irradiation. The XRD data show no signs of structural alterations, even at the highest fluences of 4×10^{13} ions/cm^2, confirming that the Ca ion irradiation does not induce a phase change. Interestingly, the $P-V$ measurements reveal an increase in both P_R and P_S values with rising fluence. Despite the annealing

TABLE 2 | Remanent (P_R) and saturation (P_S) polarization HZO at various fluences of Ca ion irradiation before and after 10.000 cycles.

Material	Fluence (ions/cm^2)	Condition	P_R (μC/cm^2)	P_S (μC/cm^2)
HZO	Reference	Pristine	3.5	8.9
		After 10^4 Cycles	4.7	10.1
	5×10^{11}	Pristine	4.9	11.1
	After 10^4 cycles	5.8	12.0	
	5×10^{12}	Pristine	6.1	12.8
		After 10^4 Cycles	6.2	12.9
	4×10^{13}	Pristine	8.6	16.5
		After 10^4 Cycles	10.3	17.6

procedure at 400°C for 1 h prior to irradiation, the film may still contain amorphous regions that crystallize under ion exposure. According to the *P*−*V* characteristics, the 10.000 wake-up cycles have less influence on the ferroelectric properties compared to samples exposed to Au ions. The inability to reverse this process through E-field cycling is attributed to the absence of the non-polar phase. These findings demonstrate the resilience of ferroelectric HZO films against light ion irradiation even at fluences as high as 4×10^{13} ions/cm^2.

In summary, electrical and structural characterization reveals that 1.635 GeV Au ions cause structural changes in both HLO and HZO films with effects becoming more pronounced at higher fluences. In HLO, the transition to a non-polar phase is responsible for the observed reduction in P_S while grain fragmentation and the corresponding increase in grain boundaries explain the observed decrease in P_R. For all samples, up to very high fluences, post cycling leads to reopening of the P−V loops by electric-field induced transformation from the non-polar back to the polar orthorhombic phase [6]. Notably, cycling results in a higher P_S value compared to the non-irradiated reference sample, confirming that the ion beam induced polar to non-polar transition is reversible. Moreover, the post cycling can even lead to a higher amount of polar phase compared to the as-grown sample which is especially true for HLO displaying improved ferroelectric properties after post-irradiation cycling. Overall, HfO_2-based ferroelectric films have a remarkable resilience to swift heavy ion irradiation. Especially the HZO samples exhibit outstanding stability maintaining good electrical performance up to fluences of 7×10^{12} ions/cm^2 of Au ion irradiation.

4 | Conclusions

Our results demonstrate that the response of hafnium oxide to swift heavy ion irradiation is influenced by its crystal structure and doping. We have shown that stoichiometric amorphous hafnium oxide can crystallize and simultaneously undergo a phase transition to rhombohedral HfO_{2-x} when irradiated with high-energy Au ions. In contrast, although Ca also induce crystallization, their lower energy loss is insufficient to trigger a phase transition. In ferroelectric HLO, Au ion irradiation leads to severe grain fragmentation, while HZO displays exceptional tolerance, maintaining stable ferroelectric properties even at fluences up to 7×10^{12} ions/cm^2. For both materials, electrical cycling after irradiation reopens the P−V hysteresis loops indicating a field-induced recovery of the polar orthorhombic phase. These findings contribute to a more comprehensive understanding of how hafnium oxide films behave under exposure to high-energy light and heavy ions. Light ion species such as Ca deposit less energy along their trajectories and have a much milder impact on structural integrity and functional performance sine no phase transition occurs. MFM capacitors, which are known to be highly sensitive to phase stability, exhibits minimal degradation when exposed to irradiation with an energy loss below the phase transition threshold. Using Au ions for the irradiation experiments, represents a worst-case scenario, because space missions are mainly exposed to protons and light ions. Our results confirm that Ca ions cause significantly less damage and that even under harsh Au irradiation HZO films retain good ferroelectric performance at very high fluences. Overall, this makes hafnium oxide an excellent candidate for non-volatile memories with applications in space or other high-dose environments where robust resilience to radiation is required.

Acknowledgements

Funding was received within the ECSEL Joint Undertaking projects WAKeMeUP and StorAIge in collaboration with the European Union's H2020 Framework Program (H2020/2014-2020) and National Authorities, under grant agreement number 783176 and 101007321, respectively. Funding by the Federal Ministry of Education and Research (BMBF) under contracts 16ESE0298, 16MEE0154 and 16ME0908K (MACHAME) is gratefully acknowledged. Also, this work was supported by the DFG grant 560/27-1. The results presented here are based on a UMAT experiment, which was performed at the X0-and M3-beamline of the UNILAC at the GSI Helmholtzzentrum für Schwerionenforschung, Darmstadt (Germany) in the frame of FAIR Phase-0.

Funding

ECSEL Joint Undertaking Project StorAIge in Collaboration With the European Union's H2020 Framework Program (H2020/2014-2020) and National Authorities, Under Grant Agreement Number 101007321. Funding by the Federal Ministry of Education and Research (BMBF) Under Contracts 16ESE0298 and 16MEE0154, and 16ME0908K (MACHAME). Funding by the DFG Grant AL 560/27-1.

Conflicts of Interest

The authors declare no conflicts of interest.

Data Availability Statement

The data that support the findings of this study are available from the corresponding author upon reasonable request.

References

1. S. U. Sharath, S. Vogel, L. Molina-Luna, et al., "Control of Switching Modes and Conductance Quantization in Oxygen Engineered HfO X Based Memristive Devices," *Advanced Functional Materials* 27 (2017): 1700432, https://doi.org/10.1002/adfm.201700432.

2. S. Petzold, A. Zintler, R. Eilhardt, et al., "Forming-Free Grain Boundary Engineered Hafnium Oxide Resistive Random Access Memory Devices," *Advanced Electronic Materials* 5 (2019): 1900484, https://doi.org/10.1002/aelm.201900484.

3. R. Winkler, A. Zintler, S. Petzold, et al., "Controlling the Formation of Conductive Pathways in Memristive Devices," *Advanced Science* 9 (2022): 2201806.

4. R. Winkler, A. Zintler, O. Recalde-Benitez, et al., "Texture Transfer in Dielectric Layers via Nanocrystalline Networks: Insights from in Situ 4D-STEM," *Nano Letters* 24 (2024): 2998–3004.

5. P. Schreyer, N. Kaiser, D. Nasiou, et al., "All HfO X -Resistive Switches with the Conducting Oxygen Vacancy Exchange Layer and Self-Limited Oxide Layer," *ACS Applied Materials & Interfaces* 17 (2025): 57632, https://doi.org/10.1021/acsami.5c12938.

6. M. Lederer, T. Vogel, T. Kämpfe, et al., "Heavy Ion Irradiation Induced Phase Transitions and Their Impact on the Switching Behavior of Ferroelectric hafnia," *Journal of Applied Physics* 132 (2022): 064102, https://doi.org/10.1063/5.0098953.

7. T. Ali, P. Polakowski, K. Kühnel, et al., "A Multilevel FeFET Memory Device Based on Laminated HSO and HZO Ferroelectric Layers for High-Density Storage,"In *2019 IEEE International Electron Devices Meeting (IEDM)* (IEEE, San Francisco, CA, USA 2019): 28.7.1–28.7.4.

8. T. Mikolajick, U. Schroeder, and S. Slesazeck, "The Case for Ferroelectrics in Future Memory Devices," *2021 5th IEEE Electron Devices Technology & Manufacturing Conference (EDTM)*, (IEEE, Chengdu, China 2021): 1–3.

9. D. Lehninger, F. Müller, Y. Raffel, et al., "Ferroelectric Hafnium Oxide: a Potential Game-Changer for Nanoelectronic Devices and Systems," *Advanced Electronic Materials* 11 (2025): 2400686, https://doi.org/10.1002/aelm.202400686.

10. D. Lehninger, R. Hoffmann, A. Sünbül, et al., "Ferroelectric FETs with Separated Capacitor in the Back-End-of-Line: Role of the Capacitance Ratio," *IEEE Electron Device Letters* 43 (2022): 1866, https://doi.org/10.1109/LED.2022.3204360.

11. D. Lehninger, M. Lederer, T. Ali, T. Kämpfe, K. Mertens, and K. Seidel, "Enabling Ferroelectric Memories in BEoL-Toward Advanced Neuromorphic Computing Architectures," In *2021 IEEE International Interconnect Technology Conference (IITC)* (IEEE, Kyoto, Japan 2021): 1–4.

12. K. Seidel, D. Lehninger, S. Abdulazhanov, et al., "A Ferroelectric BEoL Module: Adding Non-Volatile Memories and Varactors to Existing Technology Nodes," In *2023 IEEE International Interconnect Technology Conference (IITC) and IEEE Materials for Advanced Metallization Conference (MAM)(IITC/MAM)* (IEEE, Dresden, Germany 2023): 1–3.

13. S. U. Sharath, T. Bertaud, J. Kurian, et al., "Toward Forming-free Resistive Switching in Oxygen Engineered HfO2−X," *Applied Physics Letters* 104 (2014): 063502, https://doi.org/10.1063/1.4864653.

14. S. Petzold, E. Miranda, S. U. Sharath, et al., "Analysis and Simulation of the Multiple Resistive Switching Modes Occurring in HfO X -based Resistive Random Access Memories Using Memdiodes," *Journal of Applied Physics* 125 (2019): 234503, https://doi.org/10.1063/1.5094864.

15. R. Waser, *Nanoelectronics and Information Technology: Advanced Electronic Materials and Novel Devices*, (John Wiley & Sons, 2012).

16. R. Waser, R. Dittmann, G. Staikov, and K. Szot, "Redox-Based Resistive Switching Memories—Nanoionic Mechanisms, Prospects, and Challenges," *Advanced Materials* 21 (2009): 2632–2663, https://doi.org/10.1002/adma.200900375.

17. P. E. Dodd, M. R. Shaneyfelt, J. R. Schwank, and J. A. Felix, "Current and Future Challenges in Radiation Effects on CMOS Electronics," *IEEE Transactions on Nuclear Science* 57 (2010): 1747–1763, https://doi.org/10.1109/TNS.2010.2042613.

18. S. Gerardin, M. Bagatin, A. Paccagnella, et al., "Radiation Effects in Flash Memories," *IEEE Transactions on Nuclear Science* 60 (2013): 1953–1999, https://doi.org/10.1109/TNS.2013.2254497.

19. T. Vogel, A. Zintler, N. Kaiser, et al., "Structural and Electrical Response of Emerging Memories Exposed to Heavy Ion Radiation," *ACS Nano* 16 (2022): 14463, https://doi.org/10.1021/acsnano.2c04841.

20. T. Vogel, N. Kaiser, S. Petzold, et al., "Defect-Induced Phase Transition in Hafnium Oxide Thin Films: Comparing Heavy Ion Irradiation and Oxygen-Engineering Effects," *IEEE Transactions on Nuclear Science* 68 (2021): 1542–1547, https://doi.org/10.1109/TNS.2021.3085962.

21. S. Petzold, S. U. Sharath, J. Lemke, E. Hildebrandt, C. Trautmann, and L. Alff, "Heavy Ion Radiation Effects on Hafnium Oxide-Based Resistive Random Access Memory," *IEEE Transactions on Nuclear Science* 66 (2019): 1715–1718, https://doi.org/10.1109/TNS.2019.2908637.

22. R. Fang, Y. Gonzalez Velo, W. Chen, et al., "Total Ionizing Dose Effect of γ-ray Radiation on the Switching Characteristics and Filament Stability of HfOx Resistive Random Access Memory," *Applied Physics Letters* 104 (2014): 183507, https://doi.org/10.1063/1.4875748.

23. J. S. Bi, Z. S. Han, E. X. Zhang, et al., "The Impact of X-Ray and Proton Irradiation on ${\rm HfO}_2/{\rm Hf}$-Based Bipolar Resistive Memories," *IEEE Transactions on Nuclear Science* 60 (2013): 4540–4546, https://doi.org/10.1109/TNS.2013.2289369.

24. M. Alayan, M. Bagatin, S. Gerardin, et al., "Experimental and Simulation Studies of the Effects of Heavy-Ion Irradiation on HfO 2-based RRAM Cells," *IEEE Transactions on Nuclear Science* 64 (2017): 2038–2045.

25. A. L. Serra, T. Vogel, G. Lefevre, et al., "Heavy Ions Radiation Effects on 4kb Phase-Change Memory," In *2020 20th European Conference on Radiation and Its Effects on Components and Systems (RADECS)* (IEEE, Toulouse, France 2020): 1–4.

26. X. He, W. Wang, B. Butcher, S. Tanachutiwat, and R. E. Geer, "Superior TID Hardness in TiN/HfO${}_{2}$/TiN ReRAMs after Proton Radiation," *IEEE Transactions on Nuclear Science* 59 (2012): 2550–2555, https://doi.org/10.1109/TNS.2012.2208480.

27. S. L. Weeden-Wright, W. G. Bennett, N. C. Hooten, et al., "TID and Displacement Damage Resilience of 1T1R <Formula Formulatype="Inline"><Tex Notation="TeX">${\rm HfO}_2/{\rm Hf}$</Tex></Formula> Resistive Memories," *IEEE Transactions on Nuclear Science* 61 (2014): 2972–2978, https://doi.org/10.1109/TNS.2014.2362538.

28. M. J. Marinella, S. M. Dalton, P. R. Mickel, et al., "Initial Assessment of the Effects of Radiation on the Electrical Characteristics of ${\rm TaO}_{\rm X}$ Memristive Memories," *IEEE Transactions on Nuclear Science* 59 (2012): 2987–2994, https://doi.org/10.1109/TNS.2012.2224377.

29. Y. Wang, F. Huang, Y. Hu, et al., "Proton Radiation Effects on Y-Doped HfO 2 -Based Ferroelectric Memory," *IEEE Electron Device Letters* 39 (2018): 823–826, https://doi.org/10.1109/LED.2018.2831784.

30. S. Hu, Y. Liu, T. Chen, et al., "γ-Ray Radiation Effects on an HfO 2 -Based Resistive Memory Device," *IEEE Transactions on Nanotechnology* 17 (2018): 61–64, https://doi.org/10.1109/TNANO.2017.2661818.

31. X. He and R. E. Geer, "Heavy Ion Radiation Effects on TiN/HfO 2/W Resistive Random Access Memory," In *2013 IEEE Aerospace Conference* (IEEE, Big Sky, MT, USA 2013): 1–7.

32. W. M. Tong, J. J. Yang, P. J. Kuekes, et al., "Radiation Hardness of ${\rm TiO}_{2}$ Memristive Junctions," *IEEE Transactions on Nuclear Science* 57 (2010): 1640–1643, https://doi.org/10.1109/TNS.2010.2045768.

33. S. H. Chang, J. Kim, C. Phatak, et al., "X-ray Irradiation Induced Reversible Resistance Change in Pt/TiO 2 /Pt Cells," *ACS Nano* 8 (2014): 1584–1589, https://doi.org/10.1021/nn405867p.

34. N. Arun, L. D. V. Sangani, K. Vinod Kumar, et al., "Effects of Swift Heavy Ion Irradiation on the Performance of HfO2-Based Resistive Random Access Memory Devices," *Journal of Materials Science: Materials in Electronics* 32 (2021): 2973–2986.

35. J. L. Pacheco, D. L. Perry, D. R. Hughart, M. Marinella, and E. Bielejec, "Electroforming-free TaOx Memristors Using Focused Ion Beam Irradiations," *Applied Physics A* 124 (2018): 626, https://doi.org/10.1007/s00339-018-2041-3.

36. A. Benyagoub, "Evidence of an Ion-Beam Induced Crystalline-to-Crystalline Phase Transformation in Hafnia," *The European Physical Journal B—Condensed Matter* 34 (2003): 395–398.

37. A. Benyagoub, "Swift Heavy Ion Induced Crystalline-to-crystalline Phase Transition in Zirconia and Hafnia: a Comparative Study," *Nuclear Instruments and Methods in Physics Research Section B: Beam Interactions with Materials and Atoms* 218 (2004): 451–456, https://doi.org/10.1016/j.nimb.2003.12.046.

38. A. Benyagoub, "Mechanism of the Monoclinic-to-tetragonal Phase Transition Induced in zirconia and hafnia by Swift Heavy Ions," *Physical Review B* 72 (2005): 094114, https://doi.org/10.1103/PhysRevB.72.094114.

39. A. Benyagoub, "Phase Stability of the Two Isomorphs Monoclinic Zirconia and hafnia under MeV Ion Irradiation," *Acta Materialia* 60 (2012): 5662–5669, https://doi.org/10.1016/j.actamat.2012.06.030.

40. M. Lang, F. Djurabekova, N. Medvedev, M. Toulemonde, and C. Trautmann, 2020, pp. 485–516.

41. B. Schuster, F. Fujara, B. Merk, R. Neumann, T. Seidl, and C. Trautmann, "Response Behavior of ZrO2 under Swift Heavy Ion Irradiation with and without External Pressure," *Nuclear Instruments and Methods in Physics Research Section B: Beam Interactions with Materials and Atoms* 277 (2012): 45–52, https://doi.org/10.1016/j.nimb.2011.12.060.

42. W. J. Weber, "Models and Mechanisms of Irradiation-induced Amorphization in Ceramics," *Nuclear Instruments and Methods in Physics Research Section B: Beam Interactions with Materials and Atoms* 166-167 (2000): 98–106, https://doi.org/10.1016/S0168-583X(99)00643-6.

43. N. Kaiser, Y.-J. Song, T. Vogel, et al., "Crystal and Electronic Structure of Oxygen Vacancy Stabilized Rhombohedral Hafnium Oxide," *ACS Applied Electronic Materials* 5 (2023): 754–763.

44. S. Kang, W.-S. Jang, A. N. Morozovska, et al., "Highly Enhanced Ferroelectricity in HfO 2 -based Ferroelectric Thin Film by Light Ion Bombardment," *Science* 376 (2022): 731–738, https://doi.org/10.1126/science.abk3195.

45. N. Kaiser, T. Vogel, A. Zintler, et al., "Defect-Stabilized Substoichiometric Polymorphs of Hafnium Oxide with Semiconducting Properties," *ACS Applied Materials & Interfaces* 14 (2022): 1290–1303, https://doi.org/10.1021/acsami.1c09451.

46. P. Zaumseil, "High-resolution Characterization of the Forbidden Si 200 and Si 222 Reflections," *Journal of Applied Crystallography* 48 (2015): 528–532, https://doi.org/10.1107/S1600576715004732.

47. M. Toulemonde, W. Assmann, C. Dufour, A. Meftah, and C. Trautmann, "Nanometric Transformation of the Matter by Short and Intense Electronic Excitation: Experimental Data versus Inelastic Thermal Spike Model," *Nuclear Instruments and Methods in Physics Research Section B: Beam Interactions with Materials and Atoms* 277 (2012): 28–39, https://doi.org/10.1016/j.nimb.2011.12.045.

48. M. Toulemonde, E. Paumier, and C. Dufour, "Thermal Spike Model in the Electronic Stopping Power Regime," *Radiation Effects and Defects in Solids* 126 (1993): 201, https://doi.org/10.1080/10420159308219709.

49. S. G. Mayr and R. S. Averback, "Effect of Ion Bombardment on Stress in Thin Metal Films," *Physical Review B* 68 (2003): 214105, https://doi.org/10.1103/PhysRevB.68.214105.

50. J. F. Ziegler, M. D. Ziegler, J. P. Biersack, N. Instruments, and M. in, "SRIM–The Stopping and Range of Ions in Matter (2010)," *Nuclear Instruments and Methods in Physics Research Section B: Beam Interactions with Materials and Atoms* 268 (2010): 1818–1823.

51. R. L. Puurunen, A. Delabie, S. Van Elshocht, et al., "Hafnium Oxide Films by Atomic Layer Deposition for High-κ Gate Dielectric Applications: Analysis of the Density of Nanometer-thin Films," *Applied Physics Letters* 86 (2005): 073116, https://doi.org/10.1063/1.1866219.

52. Z. Li, J. Liu, P. Zhai, et al., "Latent Reliability Degradation of Ultrathin Amorphous HfO 2 Dielectric after Heavy Ion Irradiation: the Impact of Nano-Crystallization," *IEEE Electron Device Letters* 40 (2019): 1634–1637, https://doi.org/10.1109/LED.2019.2939002.

53. M. Dhanunjaya, D. K. Avasthi, A. P. Pathak, S. A. Khan, and S. V. S. Nageswara Rao, "Grain Fragmentation and Phase Transformations in Hafnium Oxide Induced by Swift Heavy Ion Irradiation," *Applied Physics A* 124 (2018): 587, https://doi.org/10.1007/s00339-018-2000-z.

54. A. M. Walke, S. Clima, M. I. Popovici, and J. V. Houdt *2024 IEEE European Solid-State Electronics Research Conference (ESSERC)* (2024): 565–568, https://doi.org/10.1109/ESSERC62670.2024.10719525.

55. T. Song, H. Tan, R. Bachelet, G. Saint-Girons, I. Fina, and F. Sánchez, "Impact of La Concentration on Ferroelectricity of La-Doped HfO 2 Epitaxial Thin Films," *ACS Applied Electronic Materials* 3 (2021): 4809–4816, https://doi.org/10.1021/acsaelm.1c00672.

56. T. Kim, M. Major, E. Miranda, et al., "Enhanced Linear Conductance Modulation by La-Doping in HfO2-Based Memristors for Neuromorphic Applications,", *Advanced Electronic Materials* (2025): 00500.

Supporting Information

Additional supporting information can be found online in the Supporting Information section.

Supporting File: aelm70212-sup-0001-SuppMat.docx